

# Journal of Biomedical Optics

[SPIEDigitalLibrary.org/jbo](http://SPIEDigitalLibrary.org/jbo)

## **Diffuse light reflectance signals as potential indicators of loss of viability in brain tissue due to hypoxia: charge-coupled-device-based imaging and fiber-based measurement**

Satoko Kawauchi  
Izumi Nishidate  
Yoichi Uozumi  
Hiroshi Nawashiro  
Hiroshi Ashida  
Shunichi Sato

# Diffuse light reflectance signals as potential indicators of loss of viability in brain tissue due to hypoxia: charge-coupled-device-based imaging and fiber-based measurement

Satoko Kawauchi,<sup>a</sup> Izumi Nishidate,<sup>b</sup> Yoichi Uozumi,<sup>c\*</sup> Hiroshi Nawashiro,<sup>ct</sup> Hiroshi Ashida,<sup>a</sup> and Shunichi Sato<sup>a</sup>

<sup>a</sup>National Defense Medical College Research Institute, Division of Biomedical Information Sciences, 3-2 Namiki, Tokorozawa, Saitama 359-8513, Japan

<sup>b</sup>Tokyo University of Agriculture and Technology, Graduate School of Bio-Application and Systems Engineering, 2-24-16 Naka-cho, Koganei, Tokyo 184-8588, Japan

<sup>c</sup>National Defense Medical College, Department of Neurosurgery, 3-2 Namiki, Tokorozawa, Saitama 359-8513, Japan

**Abstract.** Brain tissue is highly vulnerable to ischemia/hypoxia, and real-time monitoring of its viability is important. By fiber-based measurements for rat brain, we previously observed a unique triphasic reflectance change (TRC) after a certain period of time after hypoxia. After TRC, rats could not be rescued, suggesting that TRC can be used as an indicator of loss of brain tissue viability. In this study, we investigated this diffuse-reflectance change due to hypoxia in three parts. First, we developed and validated a theoretical method to quantify changes in the absorption and reduced scattering coefficients involved in TRC. Second, we performed charge-coupled-device-based reflectance imaging of the rat brain during hypoxia followed by reoxygenation to examine spatiotemporal characteristics of the reflectance and its correlation with reversibility of brain tissue damage. Third, we made simultaneous imaging and fiber-based measurement of the reflectance for the rat to compare signals obtained by these two modalities. We observed a nontriphasic reflectance change by the imaging, and it was associated with brain tissue viability. We found that TRC measured by the fibers preceded the reflectance-signal change captured by the imaging. This time difference is attributable to the different observation depths in the brain with these two methods. © The Authors. Published by SPIE under a Creative Commons Attribution 3.0 Unported License. Distribution or reproduction of this work in whole or in part requires full attribution of the original publication, including its DOI. [DOI: [10.1117/1.JBO.18.1.015003](https://doi.org/10.1117/1.JBO.18.1.015003)]

Keywords: light scattering; anoxic depolarization; brain; tissue viability; diffuse reflectance.

Paper 12322P received May 22, 2012; revised manuscript received Dec. 10, 2012; accepted for publication Dec. 10, 2012; published online Jan. 7, 2013.

## 1 Introduction

The brain is highly vulnerable to ischemia and hypoxia, and after the onset of these events, the brain becomes functionally silent, but the condition is still reversible for a certain period of time.<sup>1</sup> During this critical time period, the brain can be rescued by appropriate treatment such as blood reperfusion, but delayed reperfusion causes severe bleeding complications. Thus, it is crucially important to know this critical time zone; however, no effective method has yet been established. In addition to the temporal aspect, spatial information on tissue viability is also important for saving the brain. In ischemic stroke, it has been shown that spreading depolarization is one of the key events that determine brain tissue survival.<sup>1-3</sup> In the infarct core, impairment of energy metabolism causes anoxic depolarization, which considerably increases energy consumption and accelerates irreversible neuronal damage. In the peri-infarct penumbra region, where tissue damage is still reversible in spite of the limited

blood flow, peri-infarct depolarization (PID) occurs, leading to energy failure and hence expansion of the infarct area.<sup>4</sup> Thus, a method for noninvasive, real-time monitoring of spatiotemporal characteristics of brain tissue viability is strongly needed.

Diffuse optical measurement is attractive for monitoring tissue viability in the brain. It can provide hemodynamic and metabolic imaging contrasts by intrinsic absorption properties.<sup>5-8</sup> In addition, viability of brain tissue is related not only to energy metabolism but also to structural integrity of the cells and organelles in the tissue.<sup>1</sup> Thus, light scattering, which is sensitive to morphological changes of cells and organelles,<sup>9</sup> can also be an indicator of tissue viability in the brain. Due to the deep penetration of light into the tissue, diffuse-reflectance measurement in the near-infrared (NIR) spectral region would be useful for monitoring these absorption and scattering signals related to brain tissue viability.

By fiber-based NIR diffuse-reflectance measurements, we previously observed a unique triphasic reflectance change (TRC) at a certain time after ischemia<sup>10</sup> or hypoxia<sup>11</sup> in rat brains. In that experiment, a pair of optical fibers was placed at the center of the right hemisphere; a few minutes after starting ischemia or hypoxia, diffuse-reflectance intensity at around 805 nm increased, decreased, and increased again; thereafter it remained at a high level by the end of the measurement.<sup>10,11</sup> The TRC was shown to be associated with anoxic depolarization (AD); cerebral adenosine triphosphate (ATP) in the rats was exhausted during TRC.<sup>12</sup> Hypoxia-reoxygenation experiments

\*Present address: Kami-iida Daiichi General Hospital, Department of Neurosurgery, 2-70 Kami-iida Kita-machi, Kita-ku, Nagoya, Aichi 462-0802, Japan.

†Present address: Tokorozawa Central Hospital, Division of Neurosurgery, 753-2 Kitaakitsu, Tokorozawa, Saitama 359-0038, Japan.

Address all correspondence to: Satoko Kawauchi, National Defense Medical College Research Institute, Division of Biomedical Information Sciences, 3-2 Namiki, Tokorozawa, Saitama 359-8513, Japan. Tel: +81-4-2995-1384; Fax: +81-4-2991-1757; E-mail: [skawauch@ndmc.ac.jp](mailto:skawauch@ndmc.ac.jp)

under spontaneous respiration showed that when reoxygenation was started before TRC, all rats survived, whereas no rats survived when reoxygenation was started after TRC.<sup>11</sup> Survival was probabilistic when reoxygenation was started during TRC. These observations indicate that the period of TRC can be regarded as a critical time zone for cerebral resuscitation.<sup>11</sup> However, since AD is known to be initiated focally and to expand anisotropically in the cortex,<sup>13-15</sup> we thought that spatiotemporal behaviors of the diffuse-reflectance change during TRC are important to fully understand the correlation between diffuse-reflectance change and brain tissue reversibility. In the present study, we performed NIR diffuse-reflectance imaging of the rat brain during hypoxia by using a charge-coupled-device (CCD) and examined the relationship between spatiotemporal characteristics of the diffuse-reflectance change and brain tissue reversibility. Because observation tissue depth is limited in CCD-based imaging, we also performed simultaneous fiber-based measurement for the brain, in which observation depth was changed by changing the distance between the source and detection fibers. We previously attributed the above-mentioned NIR triphasic reflectance change to the changes in light scattering based on wavelength dependence analysis of diffuse-reflectance changes (500 to 900 nm), but we did not perform quantitative estimation of the optical properties.<sup>11</sup> Thus, in the present study, we analyzed diffuse-reflectance changes, which were measured with the same fiber setup as that used previously, to quantify time-dependent changes in the absorption and reduced scattering coefficients, for which we used multiple regression analysis aided by Monte Carlo simulation (MCS). Before analyzing *in vivo* data, we validated the method based on phantom study. We also examined the effect of distance between the source and detector fibers on sensitivity to the absorption and scattering coefficients.

## 2 Materials and Methods

We performed three kinds of diffuse-reflectance measurements for rat brains during hypoxia: fiber-based measurement, CCD imaging, and the two simultaneously. Fiber-based measurement was performed with the same experimental setup as that used in our previous study<sup>11</sup> from visible to NIR spectral regions to quantify the absorption and reduced scattering coefficients involved in the previously observed NIR diffuse-reflectance change during hypoxia. CCD-based reflectance imaging was performed to examine spatiotemporal characteristics of NIR diffuse-reflectance signals. Simultaneous measurement was conducted to compare signals obtained by these two methods, in which distance between the source and detection fibers was changed. All experiments were carried out in accordance with the Guide for Laboratory Animal Facilities and Care Regulation of the National Defense Medical College, Saitama, Japan.

### 2.1 Animal Experiments

Sprague-Dawley male rats weighing 200 to 280 g were anesthetized with pentobarbital sodium (50 mg/kg animal weight) and placed in a stereotactic frame. After the head was shaved, the scalp was incised at the midline and the parietal bone was exposed. The exposed parietal bone, which was not thinned, was soaked in gently running saline to prevent changes in light scattering of the bone from drying during the experiments. Hypoxia was induced by  $N_2$  gas inhalation, for which a face-mask was used under spontaneous respiration. The body temperature was

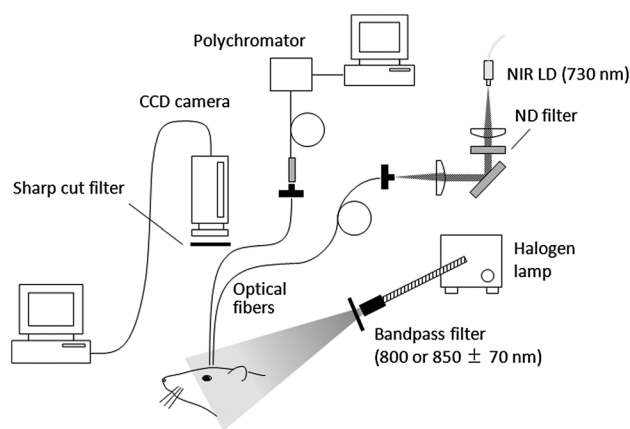


**Fig. 1** Experimental setup for CCD-based imaging and fiber-based measurement of diffuse-reflectance signal in near infrared (NIR) for a rat brain.

kept constant at  $32.0^{\circ}\text{C} \pm 0.5^{\circ}\text{C}$  by using a temperature-controlled body mat.

To perform transcranial fiber-based diffuse-reflectance measurement, a pair of 800- $\mu\text{m}$ -core-diameter optical fibers with a center-to-center separation of 2 mm, the same configuration as that used in the previous study,<sup>11</sup> was placed on the exposed parietal bone of the right hemisphere with care taken to avoid large blood vessels. A tungsten lamp (BPS120, B&W Tek, Newark, Delaware) was used as a light source with a long-wavelength-absorbing filter, which emitted broadband light from 400 to 1000 nm; the total irradiation power was set at 44  $\mu\text{W}$ . Diffuse-reflectance intensities were measured with a polychromator (PMA-11, Hamamatsu Photonics, Hamamatsu, Japan).

Figure 1 shows a diagram of the experimental setup for diffuse-reflectance imaging and simultaneous fiber-based diffuse-reflectance measurement of the rat brains. For transcranial reflectance imaging, we used illumination with NIR light that was obtained from a white light lamp (HL 100E, HOYA-Schott, Tokyo, Japan) with a bandpass filter (800  $\pm$  70 nm) for sole reflectance imaging. For simultaneous imaging and fiber measurement, the same white light lamp but with another bandpass filter (850  $\pm$  70 nm) and a 730-nm laser diode (LD) were used, respectively. For both imagings, the light was incident onto the entire cortex through the intact skull at an oblique angle to avoid specular reflection. The diffusely reflected light from the brain was imaged with an 8-bit CCD (XC-HR57, Sony, Tokyo, Japan). When fiber-based measurement was performed simultaneously, a short-wavelength cut filter (transmission,  $>780$  nm) was placed in front of the CCD to prevent detecting the 730-nm incident light. Images were acquired at 1 frame/s and stored on a personal computer using an image acquisition board (Domino Iota, Euresys, Itasca, Illinois). To clearly visualize spatiotemporal change in diffuse light reflectance, we created difference images at each time point using image acquisition and calculating software (Open eVision 1.1, Euresys, Itasca, Illinois), for which the image obtained before the occurrence of AD-related light-reflectance change was subtracted from the image obtained at each time point. Contrast of the difference images was enhanced by histogram equalization. The obtained monochromatic images were converted to false-color images by using image processing software (ImageJ, National Institutes of Health, Bethesda, Maryland).

For fiber-based diffuse-reflectance measurement with simultaneous CCD imaging, a pair of optical fibers with core diameters of 550  $\mu\text{m}$  was put on the exposed parietal bone of the right hemisphere with care taken to avoid large blood vessels. A 730-nm LD (TCLDM9, Thorlabs, Newton, New Jersey) was used as a light source, and diffuse light reflectance was measured with the same polychromator as that used in the sole fiber-based measurement; the irradiation power of the 730-nm LD was set at 2.5  $\mu\text{W}$ . To obtain depth-dependent diffuse-reflectance signal within the cerebral cortex region, the center-to-center distance of the optical fibers was changed from 1.0 to 3.0 mm. Monte Carlo simulation was performed to estimate the detectable tissue region for each fiber configuration as described below.

Before and during optical measurements, arterial oxygen saturation ( $\text{SpO}_2$ ) was monitored with a pulse oximeter (8600V, Nonin Medical, Plymouth, Minnesota), which was attached to the forelimb. After starting  $\text{N}_2$  inhalation, heartbeat was observed for about 470 s without reoxygenation. To examine the recovery of rats by reoxygenation, inhalation gas was switched from  $\text{N}_2$  to  $\text{O}_2$  at different time points after starting hypoxia under spontaneous respiration. For the rats that survived, weight and body movement were recorded for up to two weeks after reoxygenation. The relationship between spatiotemporal characteristics of diffuse-reflectance signals and reversibility of brain tissue damage was investigated. Thirty-five rats were used in the present study, divided into three large groups: 5 rats for fiber-based measurement alone, 20 rats for CCD-based reflectance imaging alone, and 10 rats for simultaneous fiber-based measurement and imaging. In the second group (imaging only), rats were subdivided into two groups: 4 rats were exposed to continuous hypoxia, and the other 16 rats were exposed to hypoxia followed by reoxygenation. The reoxygenation was started in three different time phases: early phase ( $n = 6$ ), middle phase ( $n = 5$ ), and late phase ( $n = 5$ ) during propagation of the spreading-wave-like high-reflectance region over the cortex. For the third group (simultaneous imaging and fiber measurement), three different center-to-center fiber distances were examined: 1.0 mm ( $n = 3$ ), 2.0 mm ( $n = 4$ ), and 3.0 mm ( $n = 3$ ).

## 2.2 Theoretical Analysis

To interpret changes in the diffuse-reflectance signals during hypoxia, the following two theoretical analyses were performed. One was quantification of the absorption and reduced scattering coefficients; this analysis was performed for the results of the fiber-based measurement conducted with the same experimental setup as that used in our previous study. The other was MCS to analyze optical paths of the diffusely reflected light in the tissue and its sensitivity to changes in the absorption and scattering coefficients.

### 2.2.1 Quantification of absorption coefficient and reduced scattering coefficient

To estimate the absorption and reduced scattering coefficients in rat brains, here we newly propose a modified method using multiple regression analysis aided by MCS for diffuse-reflectance spectra. The original method<sup>16</sup> can estimate absorption properties of tissue only under the assumption that the photon pathlength is independent of the tissue scattering, i.e., reduced scattering coefficient is constant. The proposed method

determines both the absorption and reduced scattering coefficients under the assumption that the photon pathlength depends on tissue scattering and the reduced scattering coefficient is variable. In the proposed method, by using the absorbance spectrum as a response variable and extinction coefficients of oxygenated hemoglobin (HbO) and deoxygenated hemoglobin (HbR) as predictor variables, the multiple regression analysis gives regression coefficients. A coefficient of scattering amplitude and the concentrations of HbO and HbR are determined from the regression coefficients using conversion vectors that have been estimated numerically in advance, by which the absorption and reduced scattering coefficients are obtained. In this study, an experimental validation study was first performed for tissue phantoms, and then quantitative estimation was carried out for rat brain *in vivo*. A detailed description of this method is presented in the next section.

**Method for quantitative estimation.** Figure 2 shows a flow chart of the proposed method. An absorbance spectrum  $A(\lambda)$  at each wavelength  $\lambda$  is defined as  $A(\lambda) = -\log_{10} R(\lambda)$ , where  $R(\lambda)$  is the diffuse-reflectance spectrum normalized by the incident light spectrum. Because attenuation due to light scattering can be treated as pseudochromophore, the absorbance spectrum  $A(\lambda)$  can be approximated as the sum of attenuations due to absorption and scattering in the brain and skull as

$$A(\lambda) = C_{\text{HbO}} I(\lambda, C_{\text{HbO}}, C_{\text{HbR}}, \mu'_s) \epsilon_{\text{HbO}}(\lambda) + C_{\text{HbR}} I(\lambda, C_{\text{HbO}}, C_{\text{HbR}}, \mu'_s) \epsilon_{\text{HbR}}(\lambda) + T(\lambda, \mu'_s) + S(\lambda), \quad (1)$$

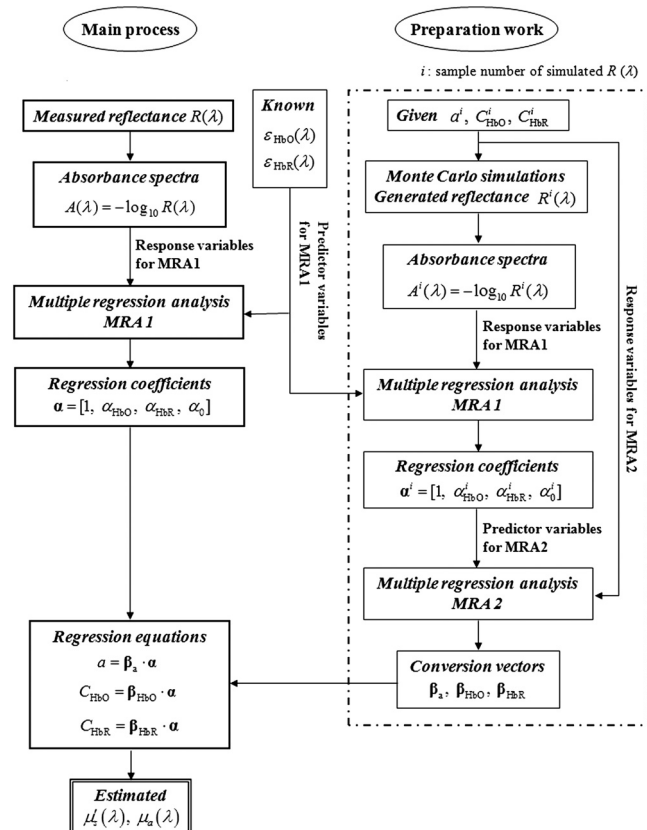


Fig. 2 Flow chart of the estimation process of the proposed method.

where  $l$  is the mean pathlength,  $T(\lambda)$  is the attenuation due to light scattering in the cortical tissue, and  $S(\lambda)$  is the attenuation due to light scattering and absorption in the skull. The absorption coefficient of the cortical tissue was assumed to depend only on the concentrations of HbO and HbR ( $C_{\text{HbO}}$ ,  $C_{\text{HbR}}$ ) as

$$\mu_a(\lambda) = C\varepsilon(\lambda) = C_{\text{HbO}}\varepsilon_{\text{HbO}}(\lambda) + C_{\text{HbR}}\varepsilon_{\text{HbR}}(\lambda). \quad (2)$$

The reduced scattering coefficient of the brain tissue was assumed to be in the following form:<sup>17</sup>

$$\mu'_s(\lambda) = a\lambda^{-b}, \quad (3)$$

where the exponent  $b$  was assumed to be constant and was given to be 1.38 using the optical properties reported in the literature.<sup>18</sup> The optical properties of the skull were assumed to be constant.

By using the absorbance spectrum  $A(\lambda)$  as a response variable and extinction coefficients  $\varepsilon_{\text{HbO}}(\lambda)$  and  $\varepsilon_{\text{HbR}}(\lambda)$  as predictor variables, multiple regression analysis based on the modified Lambert–Beer law (MRA1) was applied to Eq. (1) as

$$A(\lambda) = \alpha_{\text{HbO}}\varepsilon_{\text{HbO}}(\lambda) + \alpha_{\text{HbR}}\varepsilon_{\text{HbR}}(\lambda) + \alpha_0, \quad (4)$$

where  $\alpha_{\text{HbO}}$ ,  $\alpha_{\text{HbR}}$ , and  $\alpha_0$  are regression coefficients. The regression coefficients  $\alpha_{\text{HbO}}$  and  $\alpha_{\text{HbR}}$  describe the degree of contribution of each extinction coefficient to the absorbance spectrum and are closely related to the concentrations  $C_{\text{HbO}}$  and  $C_{\text{HbR}}$ , respectively. The regression coefficient  $\alpha_0$  is expressed as

$$\alpha_0 = \bar{A} - \bar{\varepsilon}_{\text{HbO}} \cdot \alpha_{\text{HbO}} - \bar{\varepsilon}_{\text{HbR}} \cdot \alpha_{\text{HbR}}, \quad (5)$$

where  $\bar{A}$ ,  $\bar{\varepsilon}_{\text{HbO}}$ , and  $\bar{\varepsilon}_{\text{HbR}}$  are the averages of  $A(\lambda_k)$ ,  $\varepsilon_{\text{HbO}}(\lambda_k)$ , and  $\varepsilon_{\text{HbR}}(\lambda_k)$  over the wavelength range, respectively.  $\alpha_0$  represents the bias component of  $A(\lambda)$ . Thus,  $\alpha_0$  describes the degree of contribution of the attenuation due to light scattering in the brain to the absorbance spectrum  $A(\lambda)$  and hence it is related to  $a$  in Eq. (3). At the same time,  $\alpha_0$  is also affected by absorption coefficient of the brain, since  $A(\lambda)$  is generally a function of the tissue absorption coefficient and reduced scattering coefficient.

To investigate the relationship between the regression coefficients and the values of  $C_{\text{HbO}}$ ,  $C_{\text{HbR}}$ , and  $a$ , we performed MCS for the diffuse reflectance from the rat cortical tissue through the skull at  $\lambda = 500, 520, 540, 560, 570, 580, 584, 600, 605, 730, 760, 790, 800, 805, 830,$  and  $850$  nm under the various values of  $C_{\text{HbO}}$ ,  $C_{\text{HbR}}$ , and  $a$ . We used the MCS source code developed by Wang et al.,<sup>19</sup> in which the Henyey–Greenstein phase function is applied to sampling of the scattering angle of photons. The source code was partly modified for the source-detection fiber configuration. The simulation model consisted of two layers, skull and cortical tissue, and took into account the fiber geometry used in the measurement. The source and detection areas of light were located on the boundary between the fiber end surfaces and the skull. The diameters of both the source and detection areas were 0.8 mm. The center-to-center distance between the source and detection fiber areas was 2.0 mm. In a single simulation of diffuse reflectance at each wavelength, 5,000,000 photons were randomly launched within the radius of the source area. Photons were launched with equal probability over the entire surface of the source area and were propagated into the skull and cortical tissue under the scattering and absorption. Then, some portion of the scattered light came back from the cortical tissue and, finally,

was emitted from the surface of the skull. Only photons that had an angle less than or equal to the maximum acceptance angle and passed back through the surface of detection fiber were counted into the collected light intensity. The absorption coefficients of oxyhemoglobin  $\mu_{a,\text{HbO}}$  and deoxyhemoglobin  $\mu_{a,\text{HbR}}$  were obtained from the values of  $\varepsilon_{\text{HbO}}$  and  $\varepsilon_{\text{HbR}}$  in the literature,<sup>20</sup> where the hemoglobin concentration of blood, having a 44% hematocrit with 150 g/L of hemoglobin, was converted to 100% volume concentration (100 vol.%) of hemoglobin. For the reduced scattering coefficients, the values of  $a$  were 40,172, 60,258, 80,344, and 100,430 in the simulation, which were derived by multiplying the typical value<sup>18</sup> of  $a$  by 0.5, 0.75, 1.0, and 1.25, respectively, and the reduced scattering coefficients  $\mu'_s(\lambda)$  of the cortical tissue were obtained from Eq. (3). The sum of the absorption coefficients of oxyhemoglobin and deoxyhemoglobin,  $\mu_{a,\text{HbO}} + \mu_{a,\text{HbR}}$ , represents the absorption coefficient of total hemoglobin  $\mu_{a,\text{HbT}}$ ; the values for  $C_{\text{HbT}} = 0.2, 1.0,$  and  $5.0$  vol.% were used as input to the cortical tissue in the MCS. Tissue oxygen saturation was assumed to be  $\text{StO}_2 = 60\%$  for all 12 combinations. The reduced scattering coefficient  $\mu_{s,\text{skull}}'(\lambda)$  and the absorption coefficient of the skull  $\mu_{a,\text{skull}}(\lambda)$  referred to the literature.<sup>21</sup> For all simulations, the refractive index of the fiber  $n_f$ , skull  $n_s$ , and cortical tissue  $n_c$  were fixed at 1.45, 1.5, and 1.4, respectively. The thicknesses of the skull and cortical tissue were set to be 0.35 and 4.65 mm, respectively.

Figure 3(a) and 3(b) shows the values of  $\alpha_{\text{HbO}}$  and  $\alpha_{\text{HbR}}$  versus the volume concentrations of oxyhemoglobin  $C_{\text{HbO}}$  and deoxyhemoglobin  $C_{\text{HbR}}$ , respectively, under the different conditions of  $a$ , obtained from the MCS. In Fig. 3(a), the value of  $\alpha_{\text{HbO}}$  increases with the increase of  $C_{\text{HbO}}$ . Moreover, the value of  $\alpha_{\text{HbO}}$  changes with the increase of the value of  $a$ . The same tendency is seen for  $\alpha_{\text{HbR}}$  shown in Fig. 3(b). Figure 3(c) shows the values of  $\alpha_0$  versus the values of  $a$  for the different values of  $C_{\text{HbO}}$  and  $C_{\text{HbR}}$ . The value of  $\alpha_0$  decreases with the increase of the value of  $a$ . Moreover, the value of  $\alpha_0$  increases with the increases of  $C_{\text{HbO}}$  and  $C_{\text{HbR}}$ . Therefore, it is clear that the regression coefficients  $\alpha_{\text{HbO}}$ ,  $\alpha_{\text{HbR}}$ , and  $\alpha_0$  are related to the volume concentration of oxyhemoglobin  $C_{\text{HbO}}$ , that of deoxyhemoglobin  $C_{\text{HbR}}$ , and the coefficient  $a$ , respectively; however,  $C_{\text{HbO}}$ ,  $C_{\text{HbR}}$ , and  $a$  are not determined by a unique regression coefficient when using only MRA1.

Thus, we used another multiple regression analysis, which is called MRA2, to estimate the values of  $C_{\text{HbO}}$ ,  $C_{\text{HbR}}$ , and  $a$  from the regression coefficients  $\alpha_{\text{HbO}}$ ,  $\alpha_{\text{HbR}}$ , and  $\alpha_0$  that were obtained from MRA1. In MRA2,  $C_{\text{HbO}}$ ,  $C_{\text{HbR}}$ , and  $a$  were regarded as response variables, and the three regression coefficients  $\alpha_{\text{HbO}}$ ,  $\alpha_{\text{HbR}}$ , and  $\alpha_0$  in Eq. (4) were regarded as predictor variables. Their relations are written as  $C_{\text{HbO}} = \beta_{\text{HbO}} \cdot \alpha$ ,  $C_{\text{HbR}} = \beta_{\text{HbR}} \cdot \alpha$ , and  $a = \beta_a \cdot \alpha$ , where  $\alpha = [1, \alpha_{\text{HbO}}, \alpha_{\text{HbR}}, \alpha_0]^T$ ,  $\beta_{\text{HbO}} = [\beta_{\text{HbO},0}, \beta_{\text{HbO},1}, \beta_{\text{HbO},2}, \beta_{\text{HbO},3}]$ ,  $\beta_{\text{HbR}} = [\beta_{\text{HbR},0}, \beta_{\text{HbR},1}, \beta_{\text{HbR},2}, \beta_{\text{HbR},3}]$ , and  $\beta_a = [\beta_{a,0}, \beta_{a,1}, \beta_{a,2}, \beta_{a,3}]$ . The symbol  $[\ ]^T$  represents the transposition of a vector. The coefficients  $\beta_{\text{HbO},i}$ ,  $\beta_{\text{HbR},i}$ , and  $\beta_{a,i}$  ( $i = 0, 1, 2, 3$ ) are unknown and must be determined before analysis. We adopted MCS as the foundation to establish reliable values of  $\beta_{\text{HbO},i}$ ,  $\beta_{\text{HbR},i}$ , and  $\beta_{a,i}$ . The simulation model used in this part also consisted of a skull layer and cortical tissue layer with the source-and-detection fibers geometry. The absorption coefficients  $\mu_a$  converted from the concentrations  $C_{\text{HbO}}$  and  $C_{\text{HbR}}$  and the reduced scattering coefficient  $\mu'_s$  specified by the coefficient  $a$  were provided as inputs to the simulation, while the diffuse reflectance was produced as output.

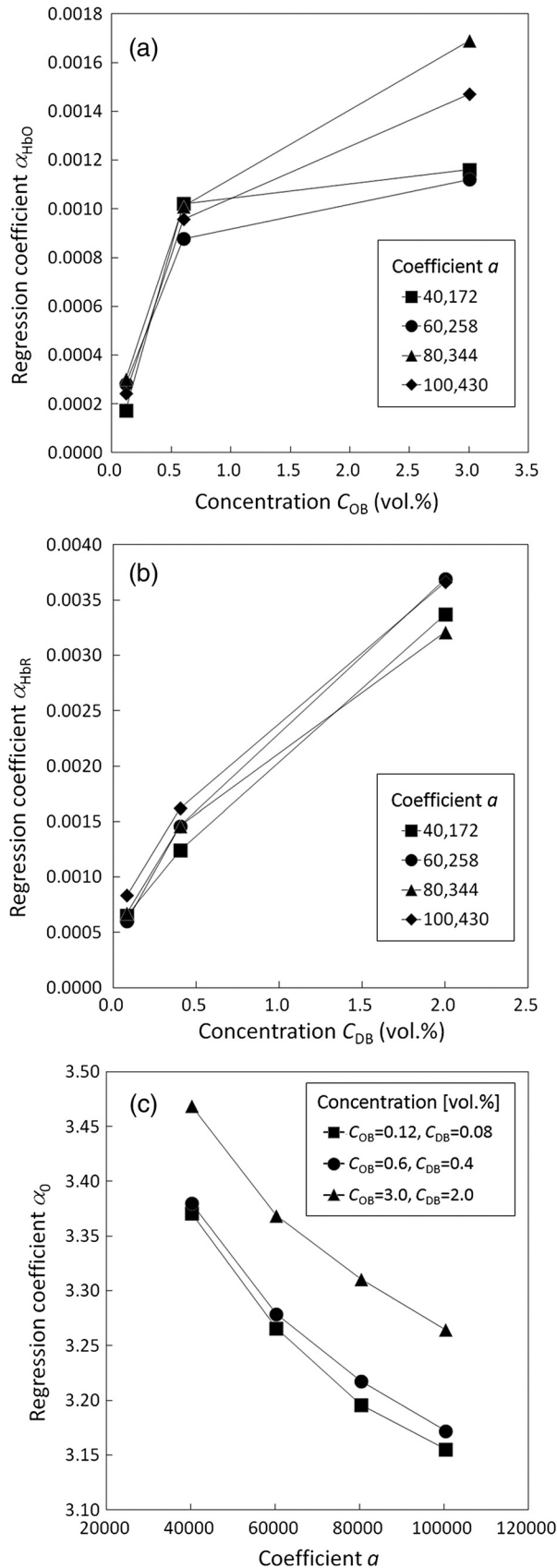


**Fig. 3** Regression coefficients versus concentrations of oxygenated and deoxygenated hemoglobins and coefficient  $a$  for scattering amplitude obtained from Monte Carlo simulation. (a) Regression coefficient  $\alpha_{HbO}$  versus concentration  $C_{HbO}$ . (b) Regression coefficient  $\alpha_{HbR}$  versus concentration  $C_{HbR}$ . (c), Regression coefficient  $\alpha_0$  versus coefficient  $a$ .

The input concentrations and coefficient  $a$  and the output reflectance are helpful as the data set in specifying the values of  $\beta_{HbO,i}$ ,  $\beta_{HbR,i}$ , and  $\beta_{a,i}$  statistically for determining the absolute concentrations and coefficient  $a$ . The five different values of 40,172, 60,258, 80,344, 100,430, and 120,516 were calculated by multiplying the typical value<sup>18</sup> of  $a$  by 0.5, 0.75, 1.0, 1.25, and 1.5, respectively, and the reduced scattering coefficients  $\mu'_s(\lambda)$  of the cortical tissue with the five different values were derived from the relation of Eq. (3). The sum of the absorption coefficients of oxyhemoglobin and deoxyhemoglobin  $\mu_{a,HbO} + \mu_{a,HbR}(\mu_{a,HbT})$  for  $C_{HbT} = 0.2, 1.0,$  and  $5.0$  vol.% were used as input to the cortical tissue in the simulation. Tissue oxygen saturation  $StO_2$  was determined by  $\mu_{a,HbO}/\mu_{a,HbT}$ , and values of 0%, 20%, 40%, 60%, 80%, and 100% were used for simulation. For the scattering and absorption properties of the skull, the refractive index of each layer, and the source and detection geometries, the same values and conditions as those described above were again employed. In total, 90 diffuse-reflectance spectra at  $\lambda = 500, 520, 540, 560, 570, 580, 584, 600, 605, 730, 760, 790, 800, 805, 830,$  and  $850$  nm were simulated under the various combinations of  $C_{HbO}$ ,  $C_{HbR}$ , and  $a$ . MRA1 for each simulated spectrum based on Eq. (4) generated the 90 sets of vector  $\alpha$  and concentrations  $C_{HbO}$ ,  $C_{HbR}$ , and  $a$ . The coefficient vectors  $\beta_{HbO}$ ,  $\beta_{HbR}$ , and  $\beta_a$  were determined statistically by performing MRA2. Once  $\beta_{HbO}$ ,  $\beta_{HbR}$ , and  $\beta_a$  were obtained,  $C_{HbO}$ ,  $C_{HbR}$ , and  $a$  were calculated from  $\alpha_{HbO}$ ,  $\alpha_{HbR}$ , and  $\alpha_0$ , which were derived from MRA1 for the measured reflectance spectrum, without the MCS. Therefore, the spectrum of absorption coefficient  $\mu_a(\lambda)$  and that of reduced scattering coefficient  $\mu'_s(\lambda)$  were reconstructed by Eqs. (2) and (3), respectively, from the measured reflectance spectrum.

*Validation using tissue phantoms.* To validate the proposed method described above, we performed experiments using tissue phantoms. The phantoms consisted of a mixture of Intralipid 10% solution (Fresenius Kabi, Sweden), oxygenated hemoglobin solution extracted from the rats, and saline solution. The compositions of the phantoms used in this study are summarized in Table 1. Optical properties of the phantoms were varied by changing concentrations of the 10%-Intralipid solution and hemoglobin solution. The reduced scattering coefficients ranged from 9.35 to 24.4  $cm^{-1}$  at the wavelengths used in the analysis to cover typical values of the cortical tissue, for which the volume percent of 10%-Intralipid solution to the total

**Table 1** Composition of the tissue phantoms (%).

Sample no.	10%-Intralipid solution	Hb solution (2.5 mmol/L)	Saline
1	10	2.8	87.2
2	15	2.8	82.2
3	10	4.2	85.8
4	15	4.2	80.8
5	10	8.3	81.7
6	15	8.3	76.7

solution was 10% or 15% on the basis of the known optical properties.<sup>22</sup> Absorption coefficients ranged from 0.12 to 7.48  $\text{cm}^{-1}$  at the same wavelengths by diluting extracted hemoglobin solution at a concentration of 2.5 mmol/L according to the measured absorbance spectra. For these phantoms, diffuse-reflectance measurements were performed with the same experimental setup as that used for *in vivo* rat brains described above. Optical fibers were contacted with the surface of solutions. The diluted hemoglobin-free 15% Intralipid solution was used as the reference sample to correct spectral characteristics of the whole measurement system. The exponent  $b$  in Eq. (3) was given as 1.04 based on the optical properties of the Intralipid solution.<sup>22</sup> Correlation between the given value of  $\mu'_s$  and estimated value of  $\mu'_s$  and that between the given value of  $\mu_a$  and estimated value of  $\mu_a$  were evaluated.

### 2.2.2 Monte Carlo simulation

For theoretical analyses other than the quantitative estimation described above, MCS was also performed on the basis of the code developed by Wang et al.<sup>19</sup> The simulation model was the same as that used in the quantitative estimation described above.

For optical properties of the skull and cerebral cortex, values reported in the literatures were used.<sup>21,23</sup> In a single simulation of diffuse reflectance, 1,000,000 photons with Gaussian distribution were launched within the radius of the source fiber. The thicknesses of the skull and cortical tissue were set to be 0.35 and 2.65 mm, respectively.

## 3 Results and Discussion

### 3.1 Quantification of Absorption Coefficient and Reduced Scattering Coefficients

#### 3.1.1 Validation using tissue phantoms

To estimate the absorption coefficient and reduced scattering coefficient of the tissue phantoms, the volume concentrations  $C_{\text{HbO}}$  and  $C_{\text{HbR}}$  and the coefficient  $a$  for scattering amplitude were determined first for the measured diffuse reflectance based on the multiple regression analysis described above. Figure 4 shows relations between the estimated and given values of the coefficient  $a$  for the scattering amplitude, volume concentration  $C_{\text{HbO}}$  for oxygenated hemoglobin,  $C_{\text{HbR}}$  for deoxygenated hemoglobin, and  $C_{\text{HbT}}$  ( $C_{\text{HbO}} + C_{\text{HbR}}$ ) for total hemoglobin. In

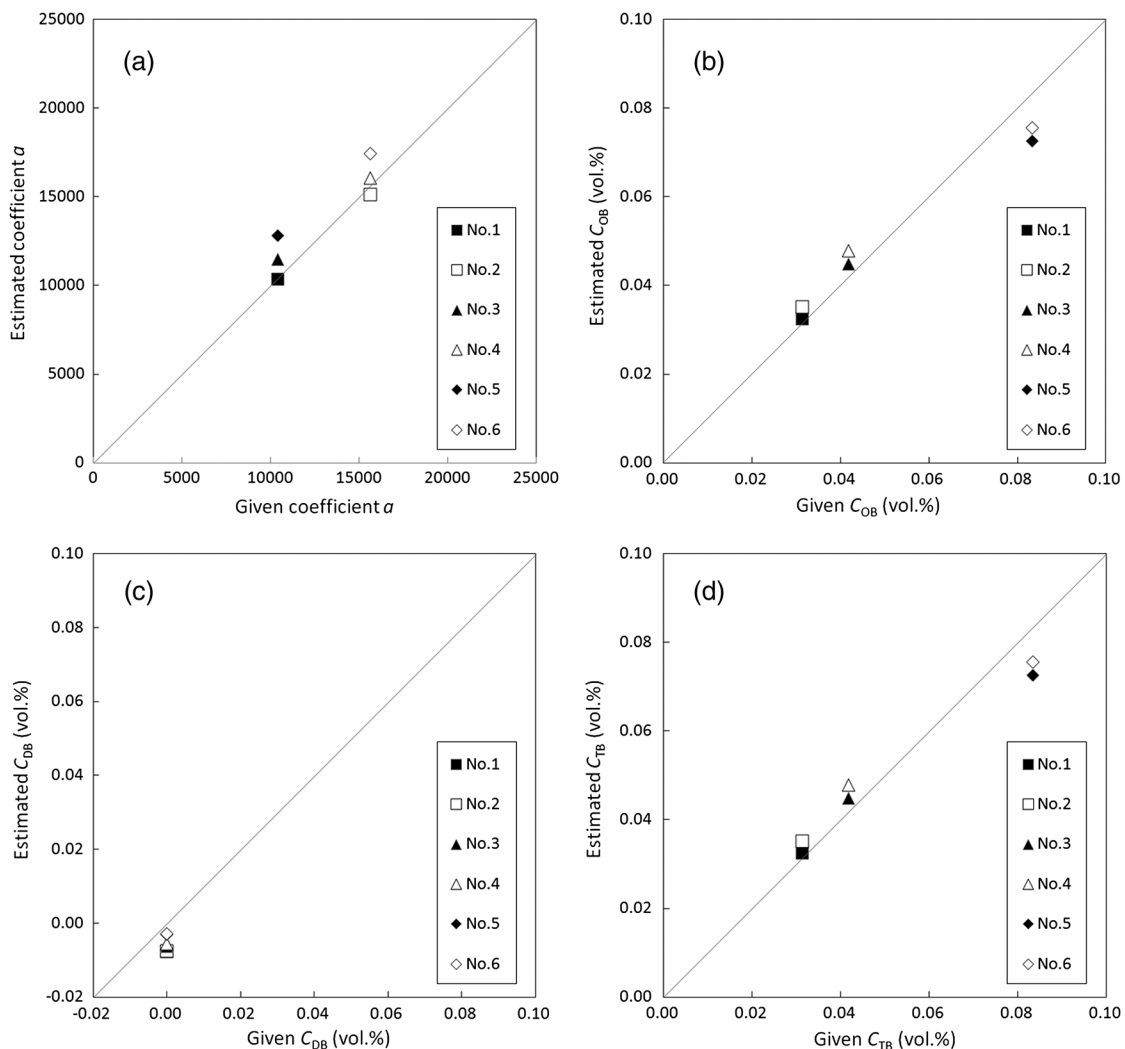


**Fig. 4** Experimental results of validation using tissue phantoms. Comparison of the estimated and given values of coefficient  $a$  for scattering amplitude (a), concentration  $C_{\text{HbO}}$  (b), concentration  $C_{\text{HbR}}$  (c), and concentration  $C_{\text{HbT}}$  (d) for tissue phantoms. Numbers 1 to 6 correspond to each sample shown in Table 1 with different coefficient  $a$  and concentration  $C_{\text{HbO}}$ .

Fig. 4(a) and 4(b), the estimated values of  $a$  and  $C_{\text{HbO}}$  well agree with the given values. In Fig. 4(c), all the estimated values of  $C_{\text{HbR}}$  are close to zero, which is consistent with the fact that the hemoglobin used in the phantoms was oxygenated hemoglobin as described above. In Fig. 4(d), a good agreement is also seen for the value of  $C_{\text{HbT}}$ , in which the value of  $C_{\text{HbR}}$  was rounded to zero when it was a negative value. These results indicate validity of the present method for estimating a coefficient  $a$  and volume concentrations  $C_{\text{HbO}}$ ,  $C_{\text{HbR}}$ , and  $C_{\text{HbT}}$  of the sample. Figure 5 shows relationships between the estimated and original values of the absorption coefficient and reduced scattering coefficient. Good agreements are seen for both coefficients. Correlation factors between the estimated and given values are 0.99 and 0.96 for the absorption and reduced scattering coefficients, respectively. Minimum and maximum differences between the estimated and given values of absorption coefficient are 4% and 15%, respectively, and those between the estimated and given values

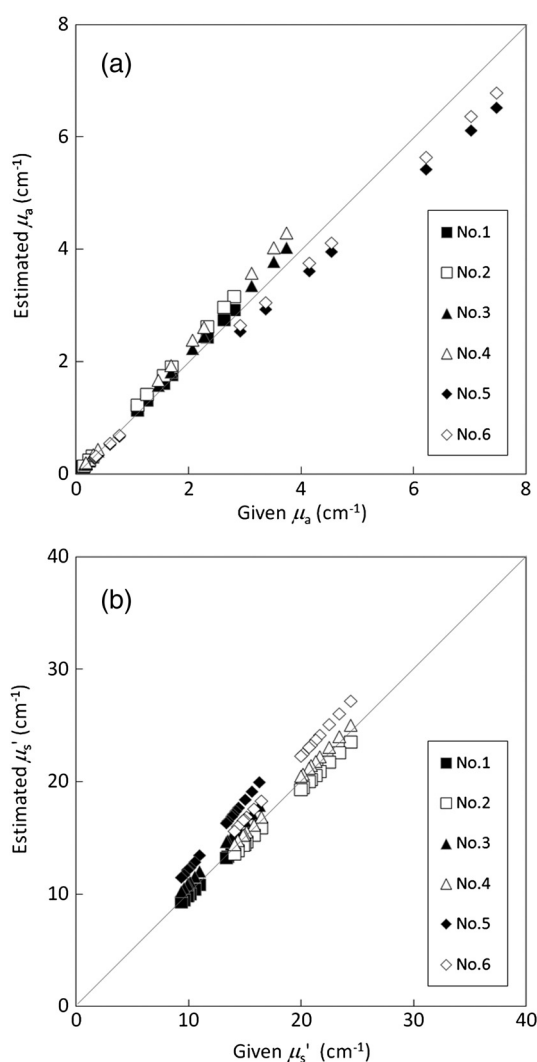


**Fig. 5** Experimental results of validation using tissue phantoms. Comparison of the estimated and given values of absorption coefficient  $\mu_a$  (a) and reduced scattering coefficient  $\mu_s'$  (b). Numbers 1 to 6 correspond to each sample shown in Table 1 with different coefficient  $a$  and concentration  $C$ . For each sample, absorption and reduced scattering coefficients at 16 different wavelengths (500, 520, 540, 560, 570, 580, 584, 600, 605, 730, 760, 790, 800, 805, 830, and 850 nm) were estimated.

of reduced scattering coefficient are 0.6% and 23%, respectively. These demonstrate the validity of the proposed method for estimating absorption and reduced scattering coefficients from the measured diffuse reflectance.

### 3.2 Quantification of Absorption and Reduced Scattering Coefficients of Rat Brain During Hypoxia

To quantify absorption and reduced scattering coefficients of the rat brain during hypoxia, we performed diffuse-reflectance measurement using the same fiber configuration as that used previously. Figure 6(a) shows time courses of the normalized diffuse-reflectance intensities at 805 and 730 nm for the rat brain during hypoxia. After starting  $N_2$  gas inhalation, the diffuse-reflectance intensity at 805 nm, which is close to an isosbestic wavelength of oxygenated and deoxygenated hemoglobins, slightly increased at  $t = 80$  s and gradually decreased for  $t = 100$  to 190 s. Thereafter, it showed a triphasic change: suddenly increased, decreased, and increased again for  $t = 190$  to 270 s, after which it gradually increased. The diffuse-reflectance intensity at 730 nm, which is a deoxygenated-hemoglobin absorption-dominant wavelength, decreased greatly immediately after starting hypoxia and thereafter showed a reflectance change similar to that observed at 805 nm. These behaviors were similar to those observed in the previous study,<sup>11</sup> and the TRC was shown to be associated with the critical time zone to rescue the brain.<sup>11</sup> For these diffuse-reflectance signals, hemoglobin concentrations ( $C_{\text{HbO}}$ ,  $C_{\text{HbR}}$ , and  $C_{\text{HbT}}$ ) and a coefficient  $a$  for the scattering amplitude were quantitatively estimated [Fig. 6(b) and 6(c)], and results of the quantification of the absorption and reduced scattering coefficients were obtained as shown in Fig. 6(d) and 6(e). It is shown that the initial reflectance decrease at 730 nm [Fig. 6(a)] is mainly caused by the absorption increase due to rapid deoxygenation, and the subsequent slight increase and gradual decrease observed at 805 and 730 nm are due to both the absorption and scattering changes [Fig. 6(d) and 6(e)], which probably reflect cellular/vascular responses to the severe hypoxia. During the following TRC [Fig. 6(a)], change in the absorption coefficient is small at both wavelengths [Fig. 6(d)], while the reduced scattering coefficients clearly show triphasic changes (increase-decrease-increase) [Fig. 6(e)]. The results of quantification were reproducible for all five rats investigated, suggesting that the TRCs shown in Fig. 6(a) are mainly due to light scattering change in the brain.

As discussed previously,<sup>11,12</sup> the triphasic scattering change is attributable to anoxic depolarization.<sup>24</sup> In AD, movements of the ions and concomitant water fluxes through the cellular membrane result in cell volume changes,<sup>25</sup> as well as changes in the distribution and structure of organelles in the tissue,<sup>26,27</sup> both leading to changes in light scattering. However, because other chromophores, such as redox centers in cytochrome c oxidase, might affect time-dependent changes in optical properties in the tissue,<sup>10</sup> further study is needed to fully understand the diffuse-reflectance changes caused by hypoxia. As described above, AD is known to have a spreading nature over the cortex, and thus, AD-related changes in optical properties in the brains may also have spatial- and temporal-dependent characteristics. We therefore performed NIR diffuse-reflectance imaging for rat brains by using a CCD and examined the validity of the diffuse-reflectance signals for monitoring brain tissue viability.

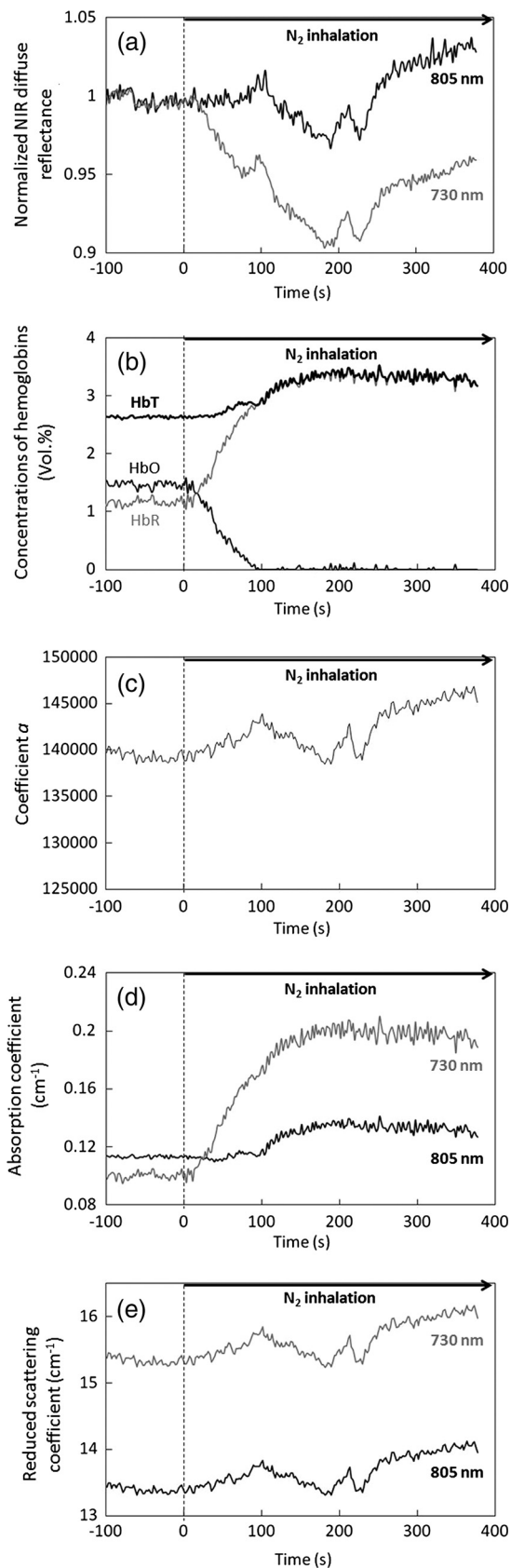


**Fig. 6** Time courses of normalized diffuse-reflectance intensities at 805 and 730 nm (a), estimated hemoglobin concentrations ( $C_{\text{HbO}}$ ,  $C_{\text{HbR}}$ , and  $C_{\text{HbT}}$ ) (b), estimated coefficient  $a$  for scattering amplitude (c), estimated absorption coefficients at 805 and 730 nm (d), and estimated reduced scattering coefficients at 805 and 730 nm (e) in a rat brain after hypoxia. Nitrogen gas inhalation was started at  $t = 0$ .

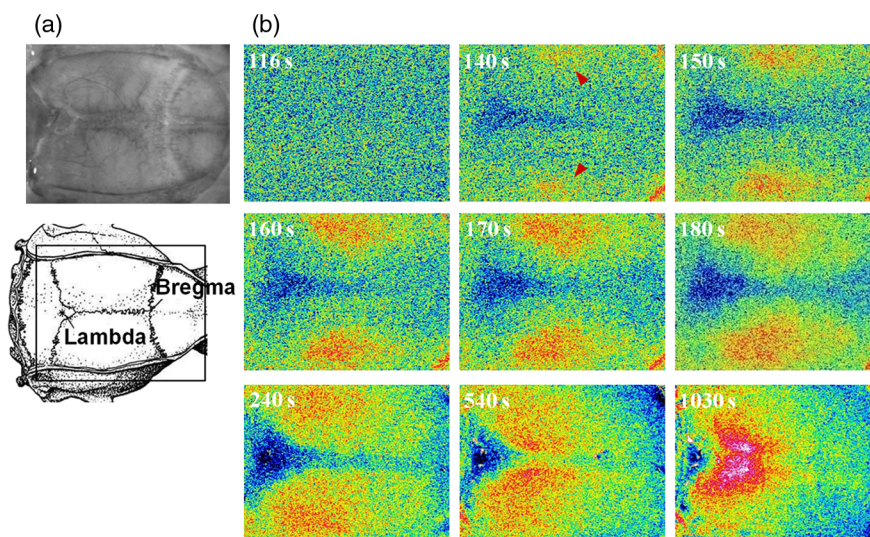
### 3.3 NIR Reflectance Imaging

Figure 7 shows typical time-course reflectance images of the rat brain after hypoxia induced by  $N_2$  gas inhalation; to create these images, the image captured before the occurrence of large diffuse-reflectance change ( $t = 115$  s) after hypoxia was subtracted from the images captured at each time point. Immediately after starting hypoxia, diffuse reflectance slightly increased and decreased for about 60 s ( $t = 0$  to 60 s) in the entire region of the cortex, and thereafter diffuse reflectance did not show any distinct change for a certain period of time (data not shown). About 130 s after starting hypoxia, diffuse reflectance increased focally in the bilateral outermost domains of the cortex [arrowheads in Fig. 7(b),  $t = 140$  s], and the regions with high diffuse reflectance spread toward the midline at a rate of about 6 mm/min [Fig. 7(b),  $t = 140$  to 240 s]. Finally, diffuse reflectance increased over the entire cortex at about 240 s or later [Fig. 7(b),  $t = 240$  to 1030 s]. We performed the same measurements for three other rats and confirmed highly reproducible spatiotemporal changes in diffuse reflectance; the regions with high diffuse reflectance were expanding over the cortex in the time range from  $t = 127 \pm 15$  s to  $t = 223 \pm 15$  s ( $n = 4$ ).

In our previous study, we observed by fiber-based diffuse-reflectance measurements that a distinct TRC started at  $128 \pm 14$  s and continued for  $64 \pm 10$  s after hypoxia;<sup>11</sup> the TRC has been shown to mainly reflect change in light scattering in the present study (Fig. 6). We performed direct current potential measurement and showed that the TRC was associated with AD,<sup>12</sup> which is known to be caused by drastic movements of ions across the cellular membrane.<sup>24</sup> Thus, the regions with high reflectance shown in Fig. 7 would also be associated with AD. Similar spreading changes of diffuse reflectance were observed for mice brains through cranial windows during ischemia with red light (635 nm) illumination.<sup>28</sup> The results shown in Fig. 7 are the first reported results showing spreading diffuse-reflectance waves in the hypoxic or anoxic rat brain with an intact skull.

To examine the relationship between spatiotemporal characteristics of the diffuse-reflectance signal and reversibility of brain tissue, we performed a hypoxia-reoxygenation experiment. Figure 8 shows diffuse-reflectance images of the rat brain that was reoxygenated after the appearance of high-reflectance regions ( $t = 171$  s); the rat survived in this case. About 140 s after starting hypoxia, diffuse reflectance increased focally in the bilateral outermost domains as seen in Fig. 7 (Fig. 8,  $t = 141$  s), and the high-reflectance regions spread toward the midline ( $t = 141$  to 161 s). We started reoxygenation when the leading edges of the high-reflectance regions had reached the middle point of the hemisphere ( $t = 171$  s). The reoxygenation suppressed the propagation of the diffuse-reflectance waves, which gradually disappeared with time ( $t = 181$  to 251 s). At a certain time after the reoxygenation, an increase in the diffuse reflectance was observed along the superior sagittal sinus ( $t = 271$  s), which is attributable to the increased cerebral blood flow due to increased energy demand of the cerebral tissue after hypoxia.

In the present study, we started reoxygenation under the three different temporal conditions and examined the survival of rats. First, when reoxygenation was started immediately after the appearance of the high-reflectance regions [Fig. 9(a)], the survival rate of rats was 67% ( $n = 6$ ). Second, when reoxygenation was started before the leading edges of the high-reflectance



**Fig. 7** (a) CCD-based NIR reflectance image of the rat brain before nitrogen gas inhalation, which was started at  $t = 0$  s. (b) Difference images of the NIR reflectances [reflectance after the onset of regional reflectance changes due to anoxic depolarization (AD) minus that before the onset of regional reflectance changes at 115 s]. Yellow-to-red colors indicate increased diffuse reflectance, and arrowheads in (b) at 140 s indicate the regions of AD generation.

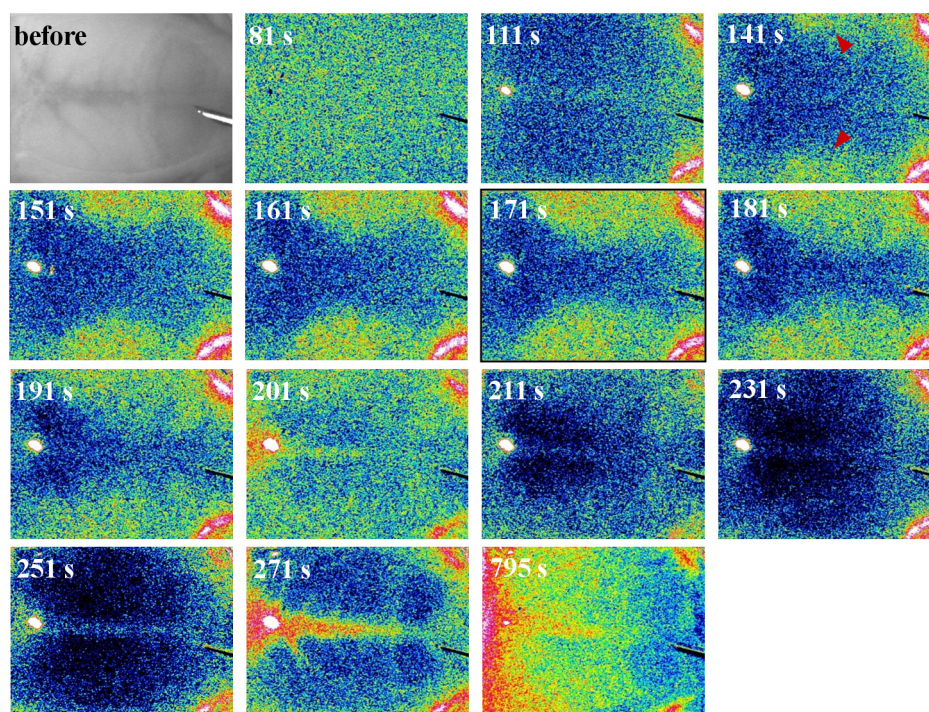


**Fig. 8** NIR reflectance image of the rat brain before nitrogen gas inhalation started at  $t = 0$  s and difference images of the NIR reflectances (reflectance after the onset of regional reflectance changes due to AD minus that before the onset of regional reflectance changes at 80 s). Yellow-to-red colors indicate increased diffuse reflectance, and arrowheads in the image at 141 s indicate the regions of AD generation. Reoxygenation was started at 171 s by switching inhalation gas from nitrogen to oxygen.

regions reached the middle point of the hemisphere [Fig. 9(b)], the survival rate of rats was 80% ( $n = 5$ ). Third, when reoxygenation was started after the high-reflectance regions had further spread and reached the midline of the brain [Fig. 9(c)], the survival rate of rats was 20% ( $n = 5$ ). These results suggest that coverage of the high-reflectance regions over the cortex is associated with reversibility of brain tissue damage. However, further study is needed to understand the probabilistic survival of rats under similar reoxygenation conditions.

### 3.4 Simultaneous Imaging and Fiber-Based Measurement of NIR Diffuse Reflectance

To compare the validities of the two optical methods for monitoring brain tissue viability, we performed CCD-based reflectance imaging and fiber-based diffuse-reflectance measurement simultaneously. Figure 10 shows typical temporal profiles of the NIR reflectance intensities obtained by the imaging [Fig. 10(a)] and fiber-based measurement (center-to-center

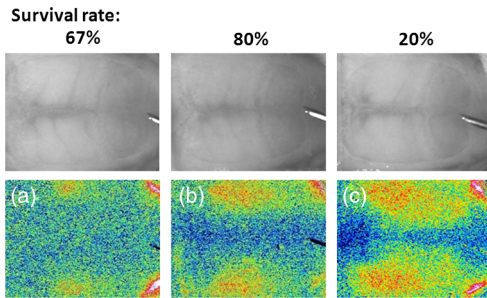


**Fig. 9** NIR difference reflectance images of hypoxic rat brains when reoxygenation was started at three different time points: (a) immediately after the appearance of high-reflectance regions (about 150 s); (b) before the leading edge of the high-reflectance regions reached the middle points of the hemispheres (about 160 s); and (c) after the high-reflectance regions had reached the midline of the brain (about 175 s) (bottom) and the corresponding field of view images (top). Survival rates of rats in each case are shown above the images.

distance of the fibers, 3.0 mm) [Fig. 10(b)]; both signals were measured from the same region of interest (ROI). Immediately after starting hypoxia, reflectance intensity obtained by imaging suddenly decreased, increased, and decreased again in the duration from 10 to 40 s and thereafter showed no distinct change for about 100 s [Fig. 10(a)]. In the same hypoxic brain model, we previously found that rapid deoxygenation occurred for about 30 s after starting hypoxia, which was followed by a large increase in cerebral blood flow for about 100 s.<sup>11</sup> The initial changes in reflectance intensity shown in Fig. 10(a) would be due to cellular and/or vascular responses to severe hypoxia. At about 150 s after hypoxia, reflectance intensity suddenly increased and this timepoint was found to coincide with the arrival time of the high-reflectance regions to the ROI for the imaging, indicating that the reflectance increase was caused by AD. The fiber-based measurement at 730 nm also showed similar temporal change of reflectance intensity (decrease-increase-decrease) in the duration from 0 to 40 s [Fig. 10(b)]. The initial intensity

decrease should reflect a rapid deoxygenation, since the illumination wavelength of 730 nm is deoxy-hemoglobin absorption dominant,<sup>20</sup> and the following increase and decrease should also be due to the change in diffuse reflectance associated with cellular/vascular responses to severe hypoxia as discussed above. Another triphasic change in the reflectance intensity (increase-decrease-increase) was observed in the duration of  $t = 100$  to 170 s, and thereafter it remained at a high level. Because TRC associated with AD has been observed by fiber-based measurements around this duration in the broad spectral region of 650 to 900 nm,<sup>11</sup> the second TRC can be regarded as being due to AD, which was also observed in the present study (Fig. 6).

Although changes in diffuse-reflectance signals associated with AD were observed with both the imaging and fiber-based measurement for the same ROI in the cortex, the AD-associated diffuse-reflectance change was not triphasic in the imaging. This difference between the two methods was reproducible for all three rats examined; one possible reason is the different observation depths of the two methods. Our Monte Carlo simulation showed that in the fiber-based measurements with a center-to-center separation of fibers of 3.0 mm [Fig. 10(b)], optical paths covered relatively deep layers of the cortex, i.e., cortical layers I to VI can be detected.<sup>29</sup> This indicates that diffuse-reflectance signals are associated with the dendrites and cerebral vasculature across all of the layers, as well as neuronal cell bodies, glial cells, and their organelles in layers II to VI. By the CCD imaging, on the other hand, the surface of the cortex probably within layers I to II/III is mainly detected, implying that reflectance signals should be dominated by dendrites and dendritic spines located in the subsurface region of the cortex as well as neurons, glia, and vasculature within layers I to II/III. To examine the depth dependence of the diffuse-reflectance signal, we performed diffuse-reflectance measurements with three different center-to-center distances of the fibers: 1.0, 2.0, and 3.0 mm. Monte Carlo simulation showed that the maximum measurement depths with these three fiber configurations were about 0.5, 1.0, and 1.5 mm, respectively, corresponding to layers I

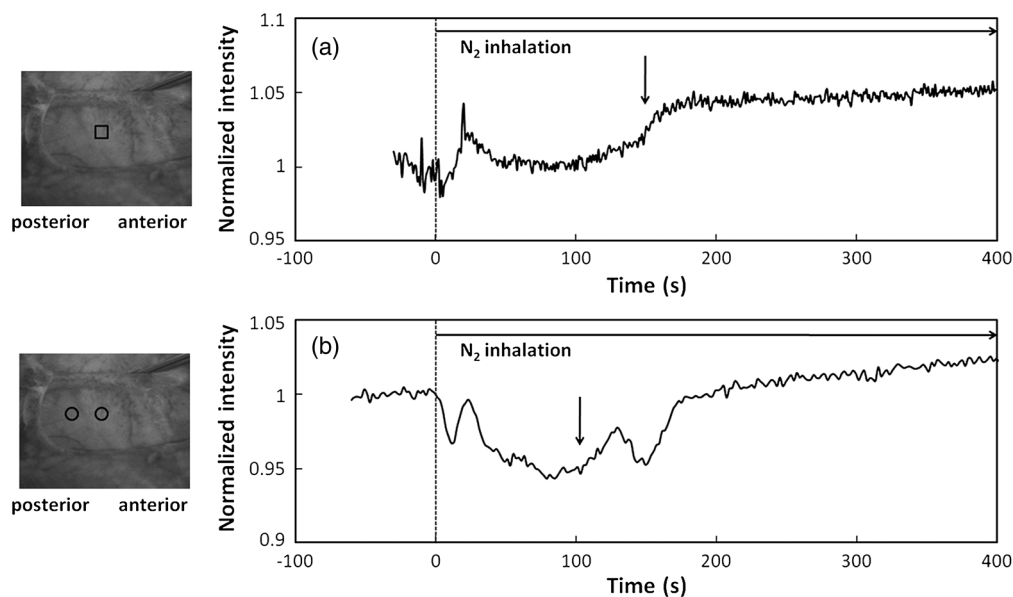


**Fig. 10** Temporal profiles of diffuse-reflectance signals obtained by the CCD-based imaging (a) and by the fiber-based measurement (b); nitrogen gas inhalation was started at  $t = 0$  s. The left images show the regions for measurements; circles in the bottom image indicate the positions of the source (right) and detector (left) fibers.

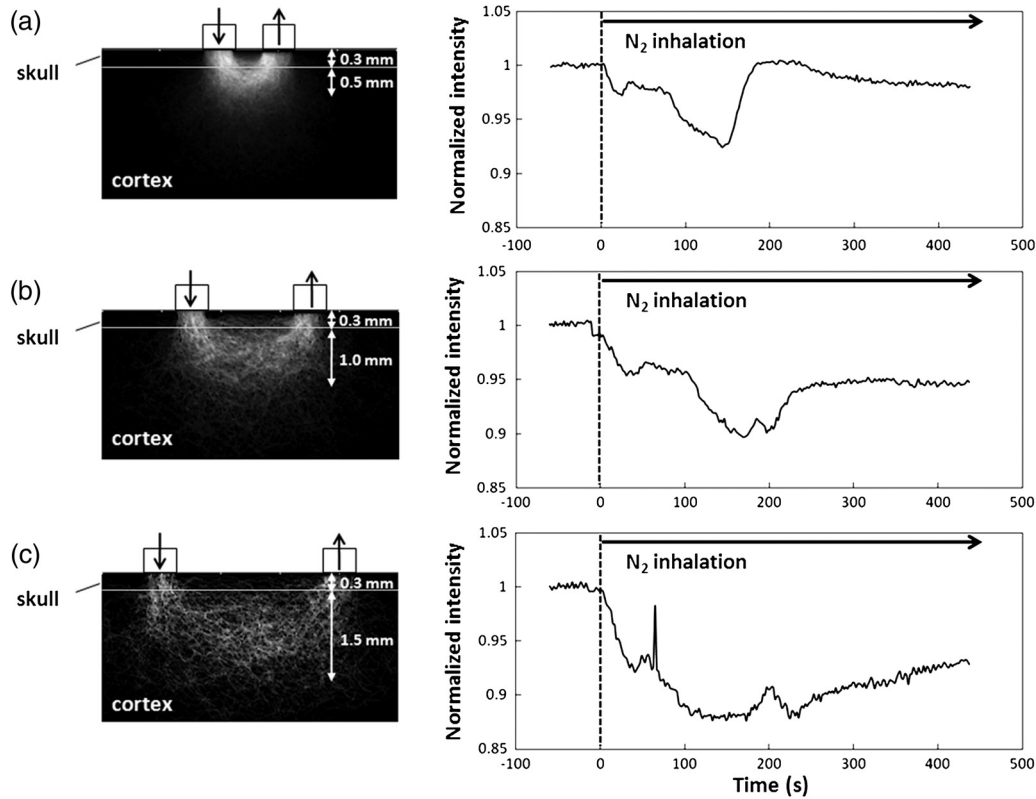


**Fig. 11** Cross-sections of the optical paths calculated by Monte Carlo simulation for the fiber-based diffuse light reflectance measurements at 730 nm (left) and time courses of the diffuse-reflectance measurements at 730 nm (right) for the three different fiber configurations; the source and detector fibers were 550  $\mu\text{m}$  in core diameter and were separated by 1.0 mm (a), 2.0 mm (b), and 3.0 mm (c). Nitrogen gas inhalation was started at  $t = 0$  s.

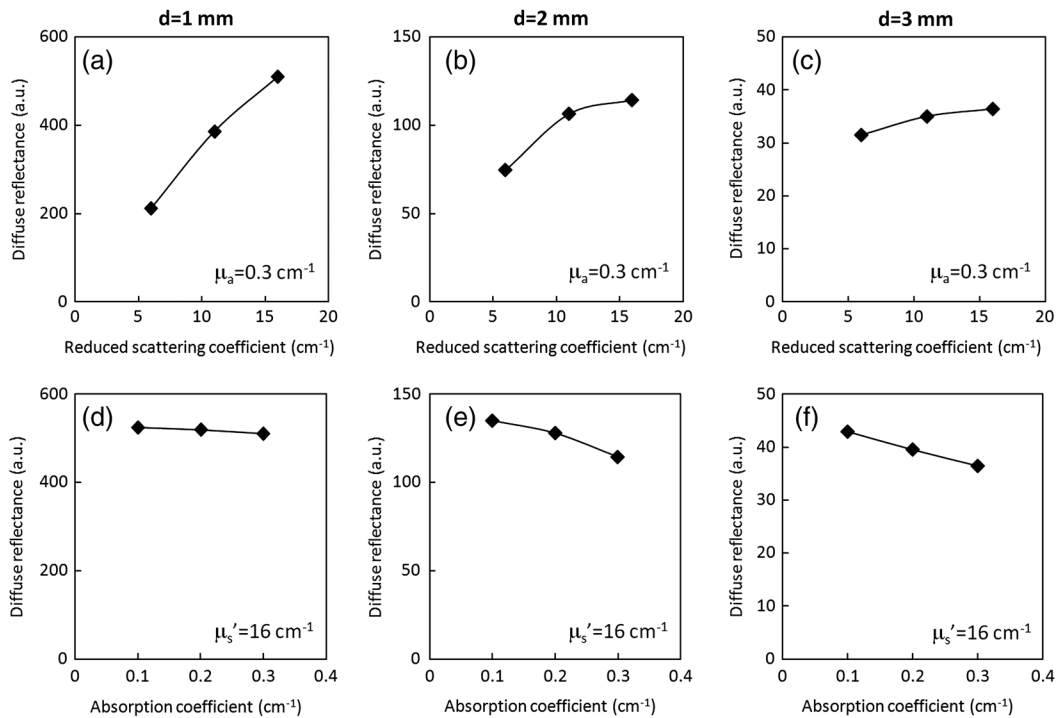


**Fig. 12** Relationships between changes in diffuse light reflectance and either reduced scattering coefficient (a)–(c) or absorption coefficient (d)–(f) for different fiber distances ( $d = 1, 2,$  and  $3$  mm) estimated by Monte Carlo simulation. In (a)–(c), absorption coefficient was constant at  $0.3 \text{ cm}^{-1}$ ; in (d)–(f), reduced scattering coefficient was constant at  $16 \text{ cm}^{-1}$ .

to III, layers I to IV or V, and layers I to V or VI in the rat cerebral cortex [Fig. 11(a) to 11(c), left]. Time courses of the diffuse light reflectance measured by these three configurations are shown in Fig. 11(a) to 11(c), right. With center-to-center distance of 1.0 mm, diffuse light reflectance showed a monotonous increase at about 150 s after hypoxia and TRC was not observed [Fig. 11(a)], whereas with center-to-center distances of 2.0 and 3.0 mm, TRC was clearly observed [Fig. 11(b) and 11(c)]. These observations were reproducible for all of the rats investigated, indicating that TRC might originate from deep layers of the cortex and TRC might not therefore be detected by the imaging.

It should be considered that the configuration of fibers, especially the distance between two fibers, can result in different sensitivities to absorption and scattering.<sup>30</sup> Figure 12 shows relationships between the diffuse light reflectance and the reduced scattering coefficient or absorption coefficient for different fiber distances, which were obtained by MCS. It is shown that diffuse reflectance measured with a distance of 1 mm [Fig. 12(a) and 12(d)] is highly sensitive to change in light scattering, while with longer fiber distances of 2 and 3 mm [Fig. 12(b)/12(c) and 12(e)/12(f)], diffuse reflectance is less sensitive to scattering change but more sensitive to absorption change. In Fig. 11, the initial reflectance decrease due to deoxygenation is larger with the longer fiber distances, which is probably due to the higher sensitivity to absorption change with the longer fiber distances. For the CCD-based imaging, the sensitivities with the distance of 1 mm [Fig. 11(a) and 11(d)] are applicable in terms of detectable depth. Thus, the reflectance change captured by the imaging would be caused mainly by change in light scattering.

It should be noted in Fig. 10 that the onset time of TRC detected by the fibers preceded the start of the monotonous increase captured by imaging. The onset time of TRC detected by fibers was  $142 \pm 37$  s, whereas the start of reflectance increase in the ROI by imaging was  $175 \pm 25$  s; the time difference between the two was  $33 \pm 12$  s. These results indicate that TRC detected by the fiber-based measurement can be an earlier signal of brain hypoxia and thus loss of brain tissue viability.

## 4 Conclusions

To examine the validity of diffuse-reflectance signals as an indicator of brain tissue viability, we performed experiments and analyses in three parts. First, we developed and validated a theoretical method to quantify changes in the absorption and reduced scattering coefficients for the measured reflectance. The quantitative estimation suggested that the NIR reflectance change was due to both the absorption and scattering changes, and the TRC more reflected light scattering change; TRC can be an indicator of loss of brain tissue viability. Further study is needed to fully understand diffuse-reflectance changes caused by hypoxia, since the current evaluation protocol included absorptions only by hemoglobins; there would be other influential chromophores, e.g., cytochrome c oxidase, to affect diffuse-reflectance changes. Second, we performed CCD-based transcranial NIR diffuse-reflectance imaging for rat brains during hypoxia to examine spatiotemporal characteristics of the reflectance signal. The results showed that regions with high diffuse reflectance were generated focally in the bilateral outermost domains in the cortex a few minutes after hypoxia and spread toward the midline at a rate of  $\sim 6$  mm/min. The survival of rats was associated with the coverage of the high-reflectance regions over the cortex. Third, we made simultaneous imaging and fiber-based measurement of the reflectance signal for the same

rat model to compare the signals obtained by these two modalities. The results showed that the reflectance signal indicating loss of brain tissue viability was not triphasic in the imaging, whereas a TRC detected by the fibers preceded the reflectance signal observed by the imaging. Such detecting time difference for the signals is attributable to the different observation depths in the brain with these two methods. These results demonstrate the usefulness of diffuse-reflectance signals to monitor loss of brain tissue viability. The tissue crisis can be detected earlier by the fiber measurement, while CCD imaging can provide two-dimensional information. Thus, the combination of CCD-based imaging and fiber-based measurement of diffuse reflectance seems to be the best option for reliable monitoring of brain tissue viability.

## Acknowledgments

The authors gratefully acknowledge the financial support, in part, of the Grant-in-Aid for Young Scientists B from Japan Society for the Promotion of Science. We thank Professor M. Kikuchi and Professor M. Ishihara for encouragement and T. Majima for technical support in the use of the image acquisition and processing software.

## References

1. K. A. Hossmann, "Viability thresholds and the penumbra of focal ischemia," *Ann. Neurol.* **36**(4), 557–565 (1994).
2. G. G. Somjen, "Mechanisms of spreading depression and hypoxic spreading depression-like depolarization," *Physiol. Rev.* **81**(3), 1065–1096 (2001).
3. M. Balestrino, "Pathophysiology of anoxic depolarization: new findings and a working hypothesis," *J. Neurosci. Methods* **59**(1), 99–103 (1995).
4. K. A. Hossmann, "Periinfarct depolarizations," *Cerebrovasc. Brain Metab. Rev.* **8**(3), 195–208 (1996).
5. F. F. Jöbsis, "Noninvasive, infrared monitoring of cerebral and myocardial oxygen sufficiency and circulatory parameters," *Science* **198**(4323), 1264–1267 (1977).
6. A. Villringer and B. Chance, "Non-invasive optical spectroscopy and imaging of human brain function," *Trends Neurosci.* **20**(10), 435–442 (1997).
7. J. P. Culver et al., "Diffuse optical tomography of cerebral blood flow, oxygenation, and metabolism in rat during focal ischemia," *J. Cereb. Blood Flow Metab.* **23**(8), 911–924 (2003).
8. P. B. Jones et al., "Simultaneous multispectral reflectance imaging and laser speckle flowmetry of cerebral blood flow and oxygen metabolism in focal cerebral ischemia," *J. Biomed. Opt.* **13**(4), 044007 (2008).
9. J. R. Mourant and I. J. Bigio, "Elastic-scattering spectroscopy and diffuse reflectance," Chapter 29 in *Biomedical Photonics Handbook*, T. Vo-Dinh, Ed., pp. 29-1–29-5, CRC Press, Boca Raton (2003).
10. S. Kawauchi et al., "Simultaneous measurement of changes in light absorption due to the reduction of cytochrome c oxidase and light scattering in rat brains during loss of tissue viability," *Appl. Opt.* **47**(22), 4164–4176 (2008).
11. S. Kawauchi et al., "Light-scattering signal may indicate critical time zone to rescue brain tissue after hypoxia," *J. Biomed. Opt.* **16**(2), 027002 (2011).
12. S. Kawauchi et al., "Light scattering change precedes loss of cerebral adenosine triphosphate in a rat global ischemic brain model," *Neurosci. Lett.* **459**(3), 152–156 (2009).
13. A. A. P. Leao, "Further observations on the spreading depression of activity in the cerebral cortex," *J. Neurophysiol.* **10**(6), 409–414 (1947).
14. P. G. Aitken et al., "Similar propagation of SD and hypoxic SD-like depolarization in rat hippocampus recorded optically and electrically," *J. Neurophysiol.* **80**(3), 1514–1521 (1998).
15. C. R. Jarvis, T. R. Anderson, and R. D. Andrew, "Anoxic depolarization mediates acute damage independent of glutamate in neocortical brain slices," *Cereb. Cortex* **11**(3), 249–259 (2001).

16. I. Nishidate, Y. Aizu, and H. Mishina, "Estimation of melanin and hemoglobin in skin tissue using multiple regression analysis aided by Monte Carlo simulation," *J. Biomed. Opt.* **9**(4), 700–710 (2004).
17. J. R. Mourant et al., "Mechanisms of light scattering from biological cells relevant to noninvasive optical-tissue diagnostics," *Appl. Opt.* **37**(16), 3586–3593 (1998).
18. V. Tuchin, *Tissue Optics: Light Scattering Methods and Instruments for Medical Diagnosis*, 2nd ed., SPIE Press, Bellingham, WA (2007).
19. L. Wang, S. L. Jacques, and L. Zheng, "MCML: Monte Carlo modeling of light transport in multi-layered tissues," *Comput. Methods Programs Biomed.* **47**(2), 131–146 (1995).
20. S. A. Prahl, "Tabulated molar extinction coefficient for hemoglobin in water," <http://omlc.ogi.edu/spectra/hemoglobin/summary.html> (1999).
21. M. Firbank et al., "Measurement of the optical properties of the skull in the wavelength range 650–950 nm," *Phys. Med. Biol.* **38**(4), 503–510 (1993).
22. H. J. van Staveren et al., "Light scattering in Intralipid-10% in the wavelength range of 400–1100 nm," *Appl. Opt.* **30**(31), 4507–4514 (1991).
23. P. van der Zee, "Measurement and modelling of the optical properties of human tissue in the near infrared," Ph.D. Thesis, University College London (1992).
24. A. J. Hansen, "Effect of anoxia on ion distribution in the brain," *Physiol. Rev.* **65**(1), 101–148 (1985).
25. T. M. Polischuk, C. R. Jarvis, and R. D. Andrew, "Intrinsic optical signaling denoting neuronal damage in response to acute excitotoxic insult by domoic acid in the hippocampal slice," *Neurobiol. Dis.* **4**(6), 423–437 (1998).
26. R. D. Andrew and B. A. MacVicar, "Imaging cell volume changes and neuronal excitation in the hippocampal slice," *Neuroscience* **62**(2), 371–383 (1994).
27. S. Bahar et al., "Mitochondrial and intrinsic optical signals imaged during hypoxia and spreading depression in rat hippocampal slices," *J. Neurophysiol.* **84**(1), 311–324 (2000).
28. T. H. Murphy et al., "Two-photon imaging of stroke onset *in vivo* reveals that NMDA-receptor independent ischemic depolarization is the major cause of rapid reversible damage to dendrites and spines," *J. Neurosci.* **28**(7), 1756–1772 (2008).
29. L. W. Swanson, "VII. Atlas of 73 transverse levels," in *Brain Maps: Structure of the Rat Brain*, L. W. Swanson, Ed., 2nd rev. ed., pp. 94–110, Elsevier, Amsterdam (1998).
30. J. S. Dam et al., "Fiber-optic probe for noninvasive real-time determination of tissue optical properties at multiple wavelengths," *Appl. Opt.* **40**(7), 1155–1164 (2001).